THE ASTROPHYSICAL JOURNAL, 225:970–987, 1978 November 1

INTENSITY AND SPECTRAL VARIABILITY OF STRONG GALACTIC X-RAY SOURCES OBSERVED BY *ANS*

D. R. PARSIGNAULT AND J. E. GRINDLAY
Harvard/Smithsonian Center for Astrophysics
Received 1978 January 5; accepted 1978 April 20

ABSTRACT

X-ray observations made by *ANS* have been used to study the spectral and intensity variations of 20 strong sources. In 15 of these sources the percentage of total power contained in 1 and 16 s time scale fluctuations varied between 2.4–8.6% and ≤4%, respectively. On time scales of 5, 15, 100, 200 minutes, 1 day, and 6 months, most of these sources showed significant intensity variations. A spectral study has shown that eight objects favor an exponential-type spectrum. Iron line emission at ~6.7 keV has been discovered from five and possibly eight of these same sources. Several objects exhibit an intensity-temperature relation similar to Sco X-1, while others are more like Cyg X-1 in their spectral variability. Comparisons of the spectra of the proposed counterparts of five X-ray bursters observed indicate that they have complex, possibly thermal, spectra which may not include iron line emission during burst activity periods. A new classification scheme is proposed for galactic-bulge sources since the spectral and temporal results suggest that these objects are either like Sco X-1 (class 1 GX sources), or like the X-ray bursters (class 2 GX sources).

Subject headings: X-rays: bursts — X-rays: sources — X-rays: spectra

I. INTRODUCTION

Several attempts have been made to classify the strong galactic X-ray sources in the galactic bulge according to their X-ray spectral distribution and intensity variations over various time scales (Cruddace *et al.* 1972; Forman, Jones, and Tananbaum 1976; Jones 1977; Ostriker 1977) or X-ray luminosities (Margon and Ostriker 1973; Canizares 1975). Several of these galactic sources have been found to be X-ray binary systems. However, most of the galactic bulge X-ray sources, despite numerous attempts at identification (e.g., Kunkel *et al.* 1970; Janes *et al.* 1972; Willmore *et al.* 1974; Mason *et al.* 1976; Markert *et al.* 1977), remain a major outstanding problem.

This paper describes the analysis of the energy spectrum and intensity fluctuations on 1 and 16 s time scales, as well as on time scales of minutes to days for 20 luminous galactic sources. We included in this group of sources several "known" source identifications for comparison purposes: Sco X-1; 4U 0614+09, which has a possible optical identification not unlike that of Sco X-1 (Davidson *et al.* 1974); 4U 1728−24, which is a slow (~122 s) pulsar (Becker *et al.* 1976); 4U 1820−30, which is the globular cluster NGC 6624 (Giacconi *et al.* 1974) and is an X-ray burster (Grindlay *et al.* 1976); and Cyg X-2 (4U 2142+38), which is a possible low-mass binary (Holt *et al.* 1976) and may be similar to Sco X-1. In addition, four other probable steady source counterparts of X-ray bursters (Lewin 1977) were included in this study: 4U 1636−53, 4U 1728−33, 4U 1735−44, and 4U 1837+04. The remaining 11 bulge sources included have no obvious identifications with other source categories. In § II we give a general description of the observations and the analysis of the time variability and spectra of the selected objects. In § III we discuss the common characteristics and the relationships to source models, and in § IV we conclude with a new suggested classification scheme for galactic-bulge X-ray sources. We describe several observational tests for the proposed GX source classification and possible models.

II. OBSERVATIONS

The Hard X-ray Experiment (HXX) on board the Astronomical Netherlands Satellite (*ANS*) observed 20 strong galactic X-ray sources (listed in Table 1, col. [1]) from 1975 February 22 until April 4, and from 1975 August 28 until October 7, with the exception of 4U 2142+38 (Cygnus X-2), which was observed 1974 December 6–13, 1975 June 5–11, and 1975 December 6–12. Three of these 20 sources, 4U 0614+09, 4U 1728−33, and 4U 1820−30, were again observed in 1976 March. In addition, observations of the Crab Nebula (4U 0531+21) were made for calibration purposes. These sources were not observed for a uniform length of time: each observing period averaged 2.4 days duration, varying from 0.10 day to 7.2 days. The frequency of the observations made on each of the sources during a given period was not spaced uniformly in time, since at a given time several sources could be visible, and an *a priori* choice had to be made as to which source to observe. The observations were made either in the "straight-pointing" mode or in the "offset-pointing" mode. In the former, the satellite points at the object

TABLE 1

MEAN X-RAY INTENSITIES AND MEASURES OF VARIABILITY FOR ALL SOURCES OBSERVED

Sources (1)	Obs. Periods JD 2,440,000.0+ (2)	Mean (counts s^{-1}) (3)	Percent rms (4)	I_{max}/I_{min} (5)	I_{max} (counts s^{-1}) (6)	Δt (day) (7)
4U 0614+09.....	2494.6–2499.1	2.4 (0.2)	28 (12)	< 2.6	2.9 (0.6)	0.52
				< 2.6	2.4 (0.5)	0.01
				< 2.4	4.2 (1.5)	0.01
	2681.5–2683.7	2.3 (0.3)	97 (43)	7.04 (5.31)	4.8 (0.7)	0.95
	2859.8–2862.9	2.2 (0.1)	24 (7)	2.85 (1.48)	2.4 (0.6)	0.13
				1.61 (0.36)	2.8 (0.4)	0.14
				1.45 (0.34)	2.6 (0.3)	0.20
				< 1.75	2.2 (0.4)	0.13
4U 1617−15						
(Sco X-1).....	2466.0–2470.1	672 (3)	6 (2)	1.56 (0.18)	859 (75)	0.43
				1.68 (0.18)	810 (50)	0.18
				1.61 (0.47)	974 (153)	0.01
				1.10 (0.01)	733 (5)	0.01
	2652.6–2654.6	762 (3)	2 (1)	1.46 (0.29)	1097 (220)	0.13
				1.41 (0.41)	1000 (272)	0.13
4U 1624−49.....	2474.2–2475.5	2.2 (0.2)	45 (32)	< 2.5	3.1 (1.0)	0.19
				2.14 (1.96)	2.3 (0.4)	0.20
	2660.0–2663.6	2.7 (0.2)	38 (24)	1.80 (0.40)	4.0 (0.6)	0.14
				< 1.9	2.4 (0.5)	1.00
4U 1636−53.....	2478.3–2478.4	< 1.5				
	2663.0–2667.0	13.9 (0.2)	28 (11)	< 1.4	15.5 (0.8)	0.94
				< 1.4	13.5 (1.1)	0.02
				> 6.5	17.1 (1.2)	0.20
4U 1642−45						
(GX 340+0).....	2477.1–2479.6	19.4 (0.1)	15 (4)	1.55 (0.11)	24.8 (1.4)	0.02
				2.51 (0.19)	38.3 (2.5)	0.33
				1.66 (0.15)	24.6 (0.7)	0.28
	2662.9–2665.5	15.3 (0.2)	9 (3)	< 1.3	17.9 (1.5)	0.01
				1.21 (0.09)	16.2 (0.8)	0.27
				1.45 (0.14)	17.6 (0.8)	0.68
4U 1658−48						
(GX 339−4).....	2482.5–2483.5	5.0 (0.7)	10 (5)	< 1.9	5.4 (1.1)	1.0
	2667.8–2668.9	2.9 (0.2)	17 (10)	< 2.9	3.2 (0.5)	0.003
				2.51 (2.51)	3.1 (0.9)	0.005
4U 1702−36						
(GX 349+2).....	2479.5–2481.0	35.5 (0.7)	26 (10)	< 1.15	32.0 (1.0)	0.20
				1.58 (0.07)	49.0 (1.4)	0.81
	2667.5–2669.0	42.3 (0.5)	33 (12)	1.69 (0.06)	57.8 (0.9)	0.06
				1.05 (0.05)	33.5 (1.6)	0.26
4U 1728−33						
(GX 354+0).....	2486.2–2487.4	6.1 (0.1)		< 1.8	4.6 (0.8)	1.0
	2670.9–2674.3	4.3 (0.3)	19 (12)	< 2.6	3.9 (1.0)	0.13
				1.87 (0.60)	4.2 (0.5)	0.80
	2850.0–2852.7	7.7 (0.1)	28 (9)	1.79 (0.33)	7.6 (0.8)	0.13
				1.37 (0.29)	7.6 (0.7)	0.40
				1.14 (0.10)	10.1 (0.6)	0.13
				< 1.30	13.9 (0.9)	0.07
4U 1728−16						
(GX 9+9).....	2484.3–2486.5	13.4 (0.2)	14 (7)	< 1.25	13.8 (0.8)	0.01
				1.54 (0.11)	16.6 (0.7)	0.20
				< 1.18	14.5 (0.5)	0.20
	2671.0–2673.7	14.7 (0.2)	7 (3)	1.17 (0.09)	15.6 (0.6)	0.14
				< 1.15	15.0 (0.6)	0.14
				1.34 (0.17)	16.0 (0.4)	0.17
4U 1728−24						
(GX 1+4).....	2485.2–2487.2	5.6 (0.7)	92 (45)	1.26 (0.26)	6.3 (0.8)	0.60
	2671.2–2673.6	2.0 (0.1)	81 (20)	1.43 (0.43)	2.7 (0.4)	0.13
				1.55 (0.37)	2.9 (0.4)	0.003
				2.14 (0.63)	2.8 (0.4)	0.006
				1.62 (0.62)	2.2 (0.5)	0.005
4U 1735−44.....	2485.9–2490.5	9.0 (0.7)	21 (10)	1.35 (0.21)	10.6 (1.1)	0.90
	2674.4–2675.9	9.4 (0.2)	11 (5)	1.25 (0.09)	10.7 (0.4)	0.53
4U 1744−26						
(GX 3+1).....	2489.3–2491.7	20.6 (0.5)	6 (3)	1.09 (0.06)	21.0 (0.8)	0.01
				1.31 (0.05)	24.2 (3.6)	0.29
	2675.7–2678.3	22.6 (0.3)	10 (5)	1.07 (0.05)	23.1 (0.5)	0.32
				1.23 (0.13)	18.9 (1.3)	0.14

TABLE 1—*Continued*

Sources (1)	Obs. Periods JD 2,440,000.0+ (2)	Mean (counts s^{-1}) (3)	Percent rms (4)	I_{max}/I_{min} (5)	I_{max} (counts s^{-1}) (6)	Δt (day) (7)
4U 1755−33						
(GX −2.5).....	2491.3–2492.5	4.0 (0.3)	45 (28)	< 1.6	4.5 (0.6)	0.004
				6.35 (6.35)	3.9 (0.8)	0.007
	2679.5–2680.8	2.9 (0.2)	24 (11)	1.95 (0.90)	4.2 (0.5)	0.14
				2.01 (2.01)	2.9 (0.8)	0.67
4U 1758−20						
(GX 9+1).....	2492.1–2495.3	32.7 (0.3)	20 (8)	1.32 (0.08)	35.0 (2.7)	0.06
				1.30 (0.03)	37.4 (1.5)	0.43
				1.51 (0.04)	43.6 (1.0)	0.80
				1.21 (0.08)	25.9 (2.3)	0.21
4U 1758−25						
(GX 5−1).....	2491.1–2495.0	60.9 (0.2)	7 (2)	1.45 (0.10)	71.2 (2.0)	0.07
				1.16 (0.06)	67.8 (2.5)	0.12
				1.24 (0.03)	67.0 (1.4)	0.48
				1.48 (0.15)	69.2 (1.1)	0.90
	2677.5–2681.1	59.2 (0.2)	9 (3)	1.19 (0.03)	65.6 (0.8)	0.14
				1.33 (0.03)	65.8 (0.8)	0.34
				1.30 (0.03)	63.9 (0.7)	0.35
4U 1811−17						
(GX 13+1).....	2495.2–2495.4	14.9 (0.4)	3 (2)	1.14 (0.04)	15.2 (0.5)	0.22
	2679.9–2683.1	14.0 (0.3)	12 (5)	1.49 (0.10)	15.9 (0.2)	0.13
				1.19 (0.09)	15.5 (1.1)	0.82
4U 1813−14						
(GX 17+2).....	2495.1–2497.7	34.4 (0.2)	19 (5)	1.11 (0.06)	32.3 (0.7)	0.005
				1.37 (0.04)	47.2 (1.0)	0.14
				2.16 (0.21)	57.5 (3.2)	0.11
	2680.9–2683.8	44.4 (0.2)	16 (7)	1.49 (0.04)	52.9 (0.6)	0.13
				1.70 (0.06)	48.7 (0.6)	0.40
4U 1820−30						
(NGC 6624).....	2495.9–2499.5	14.0 (0.2)	9 (3)	< 2.00	9.9 (1.7)	0.34
				1.28 (0.13)	15.7 (0.6)	0.18
				1.25 (0.09)	16.4 (0.6)	0.54
				< 1.60	13.3 (0.5)	0.55
	2681.9–2686.2	3.4 (0.2)	24 (8)	< 2.21	3.8 (0.7)	0.47
				< 1.66	4.5 (0.6)	0.01
				1.70 (0.63)	4.2 (0.4)	0.07
				2.56 (0.79)	3.7 (0.8)	0.01
	2860.8–2864.9	14.4 (0.1)	7 (1)	1.08 (0.05)	14.2 (0.4)	0.13
				1.11 (0.07)	15.3 (0.7)	0.66
				1.09 (0.05)	15.9 (0.4)	0.47
				1.44 (0.12)	16.1 (1.1)	0.73
				1.24 (0.08)	15.2 (0.8)	0.20
4U 1837+04						
(GX +36.3).....	2500.9–2506.5	11.4 (0.1)	14 (3)	< 1.6	8.5 (1.2)	0.01
				1.48 (0.29)	9.7 (0.5)	0.21
				1.90 (0.18)	15.9 (1.0)	0.40
				1.25 (0.08)	13.6 (0.8)	0.15
				1.17 (0.08)	14.4 (0.9)	0.01
				< 2.2	10.8 (0.9)	0.19
	2688.1–2692.7	13.8 (0.1)	13 (3)	1.27 (0.11)	17.3 (1.1)	0.20
				1.24 (0.07)	15.9 (0.5)	0.07
				1.50 (0.21)	15.1 (0.5)	0.01
				1.54 (0.12)	17.8 (1.1)	0.74
				1.50 (0.18)	16.2 (1.5)	0.81
				< 1.3	12.0 (0.6)	0.01
4U 2142+38						
(Cyg X-2).....	2387.5–2394.7	28.5 (0.2)	14 (3)	1.30 (0.16)	31.8 (2.6)	0.26
				1.63 (0.21)	40.2 (4.7)	0.05
				1.17 (0.06)	32.7 (1.1)	0.34
				1.11 (0.07)	31.7 (1.6)	0.27
				1.40 (0.10)	36.5 (1.4)	0.29
				1.23 (0.10)	24.1 (1.8)	0.29
	2568.6–2574.5	41.7 (0.2)	9 (2)	1.49 (0.13)	43.9 (2.1)	0.34
				1.08 (0.08)	43.1 (1.1)	0.06
				1.17 (0.05)	43.3 (1.1)	0.76
				1.30 (0.09)	46.3 (0.8)	0.82
				1.09 (0.06)	42.9 (0.8)	0.81
	2752.5–2758.8	26.8 (0.1)	9 (2)	1.20 (0.10)	29.1 (1.7)	0.69
				1.41 (0.12)	34.2 (2.6)	0.67
				1.32 (0.08)	27.8 (0.5)	0.29
				1.18 (0.10)	29.3 (0.5)	0.80
				1.31 (0.09)	35.0 (1.1)	0.35
				1.44 (0.12)	29.0 (1.2)	0.40

(with an accuracy of ± 0.5) for as long as $\sim 10^3$ s. In the latter mode, the instrument alternatively points at the source (with the same accuracy) for 64 s and moves away from it to a point in a suitable direction to accumulate background counts for another 64 s. X-ray fluxes were measured using the HXX Large Area Detectors (LAD) to obtain the light curves and energy spectra in the energy range 1–28 keV. A description of the HXX, its operation, and its in-flight calibration has been published elsewhere (Gursky, Schnopper, and Parsignault 1975).

a) X-Ray Time Variability

The time variability of the X-ray flux intensities from these 20 sources was studied on various time scales: 1 and 16 s, 4–9 min, 10–20 min, 80–100 min (one satellite orbit), and 180–200 min. Also, the daily variations and the variations over a 6 month period of the X-ray fluxes were observed. It was found that all of the selected X-ray sources fluctuated on the above time scales, but with different amplitudes. In many instances, the coverage of a source allowed for a periodicity search for periods of up to ~ 2 days, but no periodicities were found with modulations $\gtrsim 10\%$ (~ 3–100 s) or $\gtrsim 30\%$ (~ 2 min–2 days).

The list of observed sources is given in column (1) of Table 1. In column (2) we indicate the durations of the observing periods. The weighted averages of the X-ray fluxes for each of these periods are shown in column (3), together with the corresponding $\pm 1\,\sigma$ uncertainties. These count rates were observed in the energy range 1.4–7.2 keV. For a Crab-type spectrum, 1 *ANS* count s^{-1} in this energy band corresponds to $(3.3 \pm 1.0) \times 10^{-10}$ ergs cm^{-2} s^{-1}, or about $\sim 2.5 \times 10^{-10}$ ergs cm^{-2} s^{-1} in the 2–6 keV energy band of the *Uhuru* satellite. Thus 1 *ANS* count $s^{-1} \approx 15$ *Uhuru* counts s^{-1}. As can be seen, the observed sources covered a wide range of intensities, varying from 6.6×10^{-10} ergs cm^{-2} s^{-1} (4U 1728−24) to 2.5×10^{-7} ergs cm^{-2} s^{-1} (Sco X-1).

In column (4) of the same table, the weighted percentage rms fluctuations (and errors) for each of the time periods are indicated. This quantity is defined as

$$\%\ \text{rms} = \frac{\text{“rms”}}{\langle I \rangle} \times 100\,,$$

where $\langle I \rangle$ is the weighted mean and “rms” is the weighted rms fluctuation of the X-ray flux intensity during the given period. The source intensities used were derived from fluxes observed during all the separate pointed observations in a given observing period, so that the percentage rms fluctuation is a measure of the overall variability over the same time period. A range of percentage fluctuations was found, varying from $2 \pm 1\%$ (Sco X-1) to $81 \pm 20\%$ (4U 1728−24). Also, for several X-ray sources, this same quantity was found to vary from one observing period to the next, 6 months later. The largest changes in the percentage rms fluctuations between two adjacent observing periods were found in the case of 4U 0614+09, Sco X-1, 4U 1811−17, and 4U 1820−30, varying from $97 \pm 43\%$ to $24 \pm 7\%$, $6 \pm 2\%$ to $2 \pm 1\%$, $3 \pm 2\%$ to $12 \pm 5\%$, and $24 \pm 8\%$ to $7 \pm 1\%$, respectively. The rms fluctuations were found to be constant or almost constant between the observing periods for the remaining sources.

Finally, in columns (5), (6), and (7) respectively we show the largest ratios of the maximum to the minimum intensity (I_{max}/I_{min}) for each day the source was observed, the value of I_{max} (counts s^{-1}), and the time interval Δt (fraction of a day) during which these extremes of intensity were observed.

In Table 2, we present the results of our calculations of the percentage of the total X-ray power contained in fluctuations on 1 and 16 s time scales. For comparison, we have included the percentage power contained in 0.1 s time scale fluctuations, as observed by *Uhuru* (see Table 1 of Forman, Jones, and Tananbaum 1976). However, these authors included in each

TABLE 2

PERCENTAGE POWER IN INTENSITY FLUCTUATIONS ON 0.1, 1, AND 16 s TIME SCALES

Source	β (%) 0.1 s*	Significance (σ)	β (%) 1 s	Significance (σ)	β (%) 16 s	Significance (σ)
4U 0531+21.....	6.3 (1.2)	3.0	< 3.4	...	< 4.0	...
4U 1617−15.....	...	...	2.8 (0.3)	...	0.7 (0.2)	...
4U 1636−53.....	7.1 (3.0)	1.5	< 11.6	...	< 8.0	...
4U 1642−45.....	6.4 (1.5)	2.4	3.3 (1.4)	0.9	< 2.9	...
4U 1702−36.....	7.8 (1.1)	3.8	< 7.9	...	< 3.3	...
4U 1728−16.....	...	...	6.4 (2.4)	1.6	< 2.8	...
4U 1735−44.....	...	...	8.6 (1.7)	2.6	2.2 (1.9)	0.9
4U 1744−26.....	8.9 (1.5)	3.3	< 9.3	...	3.0 (0.6)	2.2
4U 1758−20.....	8.2 (1.1)	4.0	7.0 (2.7)	1.6	< 3.8	...
4U 1758−25.....	4.8 (1.2)	2.2	3.6 (0.6)	1.6	< 3.5	...
4U 1811−17.....	7.8 (1.8)	2.5	3.7 (1.7)	0.9	3.4 (0.7)	2.5
4U 1813−14.....	4.6 (0.7)	3.5	4.2 (0.9)	2.0	1.1 (0.7)	0.6
4U 1820−30.....	7.8 (1.9)	2.4	2.4 (1.6)	0.5	< 4.0	...
4U 1837+04.....	9.9 (2.5)	2.2	< 10.0	...	< 3.2	...
4U 2142+38.....	6.2 (1.4)	2.4	4.5 (1.4)	1.9	2.1 (0.9)	1.5

* *Uhuru* data, corrected from incorrect values given by Forman *et al.* 1976.

of their fits to the data one too many parameters. We therefore recalculated the percentage power on that time scale with the correct number of degrees of freedom. This leads to a significant reduction in the percentage power and statistical significance of the 0.1 s fluctuations observed by *Uhuru*.

Our analysis for the 1 and 16 s time scale fluctuations follows the procedure of Forman, Jones, and Tananbaum, except that we used T_i, the total observed intensity, instead of the net source intensity I_i, since in our case the background rate B is not $\ll I$. The analysis was carried out as follows: during a given observation of a source we first calculated $\langle T\rangle_{1,16}$, the average total intensity on a 1 s or 16 s integration time. We then performed χ-square fits to these constant intensities using the 1 s intensity data, or the intensity averaged in 16 s time bins. The expression for ${\chi_T}^2$ is

$$\chi_T{}^2 = \sum_i (T_i - \langle T\rangle)^2/\langle T\rangle \,.$$

It then can be shown that

$$\beta = [(\chi_\nu{}^2 - 1)/\langle T\rangle]^{1/2} \,,$$

where β is the percentage of the total power contained in 1 or 16 s time scale fluctuations and $\chi_\nu{}^2$ is the χ^2 per degree of freedom of the fits. In the columns listing the values of β, the numbers in parentheses correspond to $\pm 1\,\sigma$ uncertainties. The significance of each χ^2 fit is also indicated in the adjacent columns. The upper limits given correspond to 3 times the uncertainties in β. This analysis had to be restricted to sources with average intensities ≥ 9 counts s^{-1}, below which the χ^2 technique became insensitive.

We verified that the β values derived were not contaminated by background fluctuations by performing the identical analysis on the locally observed background, which gave β values consistent with 0%. A β analysis for source fluctuations on a 64 s time scale could not be performed since, in general, the background radiation environment varied too much over a typical 10^3 s period necessary for such calculations.

Our analysis shows that the percentage of the X-ray power fluctuating on a 1 s time scale for 15 of the sources varied between 2.4% and 8.6%; both extremes are bursters. These percentages are approximately equal to that on a 0.1 s time scale. On a 16 s time scale, the percentage of X-ray power never exceeded 4%.

In Table 3 we present the results of our analysis on the various other time scales. Columns (2) through (7) list the *maximum* ratio I_{max}/I_{min} observed for each of the sources on the time scales shown. The numbers in parentheses represent $\pm 1\,\sigma$ uncertainties. I_{max} and I_{min} were obtained by averaging the source intensity over as many adjacent 64 s blocks as possible contained in the indicated time scales. For the daily variations, the average intensities were calculated over the days starting at 0:00 UT of each day. The 4–8 min period was the shortest time scale able to yield meaningful results.

Carrying the analysis further, we calculated for each source (when at least three possible intensity ratios could be evaluated on a given time scale) the weighted averages of the I_{max}/I_{min} ratios for each of the time ranges. The results are given in Table 4. Our results first indicate that the total X-ray emission of our calibration source, the Crab Nebula, may be "variable" on several time scales considered, especially

TABLE 3

MAXIMUM INTENSITY TRANSITIONS (I_{max}/I_{min}) ON DIFFERENT TIME SCALES

Sources	4–9 min†	10–20 min	80–100 min	180–200 min	1 day	6 months
4U 0531+21	1.04 (0.02)	1.02 (0.01)	1.05 (0.02)	1.05 (0.03)	1.05 (0.01)	1.003 (0.003)
4U 0614+09	1.80 (0.80)	1.34 (0.25)	2.78 (1.32)	1.44 (0.32)	1.32 (0.19)	< 1.43
4U 1617−15	1.10 (0.01)	1.06 (0.02)	< 1.90	1.68 (0.18)	1.14 (0.05)	1.14 (0.01)
4U 1624−49	1.91 (0.72)	...	...	1.80 (0.40)	< 2.7	1.20 (0.16)
4U 1636−53	1.26 (0.11)	< 1.36*	...	> 6.6*	1.25 (0.04)*	>10
4U 1642−45	1.20 (0.05)	1.90 (0.15)	1.57 (0.11)	1.46 (0.14)	1.27 (0.02)	1.27 (0.02)
4U 1658−48	< 1.90	< 1.80	...	< 1.80*	1.33 (0.33)*	1.72 (0.28)
4U 1702−36	1.06 (0.03)*	...	1.69 (0.06)*	...	1.56 (0.06)	1.19 (0.03)
4U 1728−33	2.26 (1.2)	...	1.57 (0.26)	1.79 (0.32)	1.43 (0.08)	1.79 (0.13)
4U 1728−16	1.18 (0.09)	...	1.47 (0.09)*	1.34 (0.17)	1.06 (0.04)	1.10 (0.02)
4U 1728−24	2.14 (0.63)	...	...	1.43 (0.43)	< 1.75	2.77 (0.36)
4U 1735−44	1.18 (0.10)	< 1.30*	...	1.15 (0.08)	1.16 (0.08)	1.04 (0.04)
4U 1744−26	1.18 (0.06)	...	< 1.60*	1.23 (0.13)	1.30 (0.07)	1.10 (0.03)
4U 1755−33	< 2.10	...	...	1.41 (0.35)	1.28 (0.28)	1.38 (0.14)
4U 1758−20	1.18 (0.04)	1.17 (0.06)*	1.29 (0.09)	...	1.55 (0.07)	...
4U 1758−25	1.03 (0.03)	1.18 (0.03)	1.45 (0.10)	1.30 (0.03)	1.07 (0.01)	1.03 (0.01)
4U 1811−17	1.24 (0.14)	...	...	1.47 (0.16)	1.04 (0.04)*	1.06 (0.04)
4U 1813−14	1.17 (0.03)	1.50 (0.10)	1.99 (0.12)	2.16 (0.17)	1.32 (0.02)	1.29 (0.01)
4U 1820−30	2.56 (0.92)	1.12 (0.06)	2.28 (0.60)	1.94 (0.60)	1.68 (0.24)	4.24 (0.25)
4U 1837+04	1.32 (0.12)	1.76 (0.27)	1.35 (0.09)	1.49 (0.09)	1.31 (0.08)	1.21 (0.01)
4U 2142+38	1.23 (0.09)	1.26 (0.13)	1.63 (0.21)	1.31 (0.08)	1.50 (0.03)	1.54 (0.01)

† Time scales for maximum transition I_{max}/I_{min}.

* Only one intensity transition recorded on time scales so designated.

TABLE 4

WEIGHTED AVERAGES OF I_{max}/I_{min} ON DIFFERENT TIME SCALES

Source	4–9 min	10–20 min	80–100 min	180–200 min	1 day
4U 0531+21	1.019 (0.006)	1.016 (0.015)	1.010 (0.005)	1.009 (0.006)	1.023 (0.003)
4U 0614+09	1.15 (0.09)	1.14 (0.13)	1.15 (0.07)	1.22 (0.08)	1.11 (0.06)
4U 1617−15	1.08 (0.01)	1.06 (0.02)	1.17 (0.17)	1.26 (0.10)	1.03 (0.01)
4U 1624−49	1.25 (0.20)	...	...	1.65 (0.27)	1.70 (0.67)
4U 1636−53	1.09 (0.04)	...	...	...	...
4U 1642−45	1.09 (0.01)	1.14 (0.03)	1.19 (0.02)	1.07 (0.02)	1.15 (0.01)
4U 1658−48	1.14 (0.13)	...	...	...	...
4U 1702−36	...	...	...	...	1.50 (0.02)
4U 1728−33	1.09 (0.04)	...	1.06 (0.04)	1.15 (0.05)	1.23 (0.03)
4U 1728−16	1.10 (0.03)	...	...	1.06 (0.03)	1.03 (0.02)
4U 1728−24	1.44 (0.18)	...	...	1.43 (0.43)	1.10 (0.10)
4U 1735−44	1.16 (0.06)	...	...	1.10 (0.04)	1.13 (0.06)
4U 1744−26	1.10 (0.03)	...	...	...	1.10 (0.03)
4U 1755−33	1.18 (0.12)	...	...	1.24 (0.22)	...
4U 1758−20	1.10 (0.03)	...	1.18 (0.05)	...	1.23 (0.02)
4U 1758−25	1.02 (0.01)	1.05 (0.01)	1.09 (0.01)	1.08 (0.01)	1.03 (0.01)
4U 1811−17	1.09 (0.05)	...	...	1.13 (0.08)	...
4U 1813−14	1.05 (0.01)	1.10 (0.02)	1.11 (0.01)	1.19 (0.01)	1.17 (0.01)
4U 1820−30	1.06 (0.01)	1.11 (0.04)	1.04 (0.01)	1.03 (0.01)	1.05 (0.01)
4U 1837+04	1.07 (0.01)	1.09 (0.02)	1.10 (0.02)	1.15 (0.02)	1.07 (0.01)
4U 2142+38	1.03 (0.01)	1.05 (0.02)	1.07 (0.01)	1.07 (0.01)	1.09 (0.01)
Grand weighted averages	1.059 (0.004)	1.068 (0.007)	1.086 (0.005)	1.095 (0.005)	1.102 (0.004)

on a 4–9 min time scale (1.9 ± 0.6%), and from day to day (2.3 ± 0.3%). While this may indicate that the total minimum errors in our intensity ratio averages (Table 4) are ~2%, it is also possible that fluctuations of the Crab pulsar were detected on these time scales.

We next calculated the weighted averages (over all sources) of these average intensity ratios and compared each individual source to these weighted averages. A source was considered to be exceptionally active (or inactive) on a given time scale if the intensity ratio differed from the weighted average by $\pm 2\,\sigma$. Applying this criterion, we found that on the 4–9 min time scale, Sco X-1, 4U 1642−45, and 4U 1728−24 were very active, while 4U 1758−25 and Cyg X-2 were remarkably stable. On the 10–20 min time scale, only 4U 1642−45 was active. On the 80–100 min time scale, again 4U 1642−45 and 4U 1813−14 showed excessive variability, while 4U 1820−30 was found to be relatively constant. On the 180–200 min time scale, 4U 1642−49 and 4U 1813−14 showed large amounts of activity, while on the same time scale 4U 1820−30 and 4U 2142+38 were found to have below-average time fluctuations. On a daily time scale, large intensity fluctuations were found for 4U 1642−45, 4U 1702−36, 4U 1728−33, 4U 1758−20, and 4U 1813−14. Below-average daily fluctuations were observed for Sco X-1, 4U 1728−16, 4U 1758−25, 4U 1820−30, and 4U 1837+04.

The largest average intensity changes over a 6 month interval were found in the cases of 4U 1636−53 and 4U 1830−40, which varied from less than 1.5 counts s^{-1} (3 σ upper limit) to 13.9 ± 0.2 counts s^{-1}, and by factor 4, respectively. Also, changes greater than 50% over a 6 month period were observed in the case of 4U 1658−48, 4U 1728−33, 4U 1728−24, and 4U 2142+38. 4U 1728−16, 4U 1735−44, 4U 1744−26, 4U 1758−25, and 4U 1811−17, and especially the Crab Nebula, were found to be rather constant in intensity on the same time scale.

Finally, during each of the two observing periods on 4U 1837+04 (total exposure of 20,300 s and 15,000 s, respectively), an X-ray burst was observed. They occurred on JD 2,442,501.6956 and JD 2,442,690.6386, and were each detected for ~1–2 s. An analysis similar to that carried out for NGC 6624 was used to rule out any artifacts in the data (Grindlay *et al.* 1976). The energy flux in each burst, in the energy band of 1.4–7.2 keV, was $(7.4 \pm 2.3) \times 10^{-9}$ ergs cm^{-2} s^{-1} and $(8.2 \pm 0.3) \times 10^{-9}$ ergs cm^{-2} s^{-1}. This corresponds to a burst luminosity of ~7.4 and 8.2×10^{37} ergs s^{-1} assuming the source to be at 10 kpc distance, or somewhat less than reported by Lewin (1977).

Figures 1–6 show light curves of some of the observed sources. Each point represents the average intensity for an observation lasting between 256 and 512 s. Although some observations lasted as long as 10^3 s, it happened often that not all of the data were useful because of poor background determination. The error bars on each point represent $\pm 1\,\sigma$ statistical and aspect uncertainties folded together with the aspect corrections (cf. Gursky, Schnopper, and Parsignault 1975).

b) Spectra

Using the 15 channel logarithmic pulse height analyzer (PHA) of the LAD, we have studied the X-ray spectra of these same 20 galactic sources

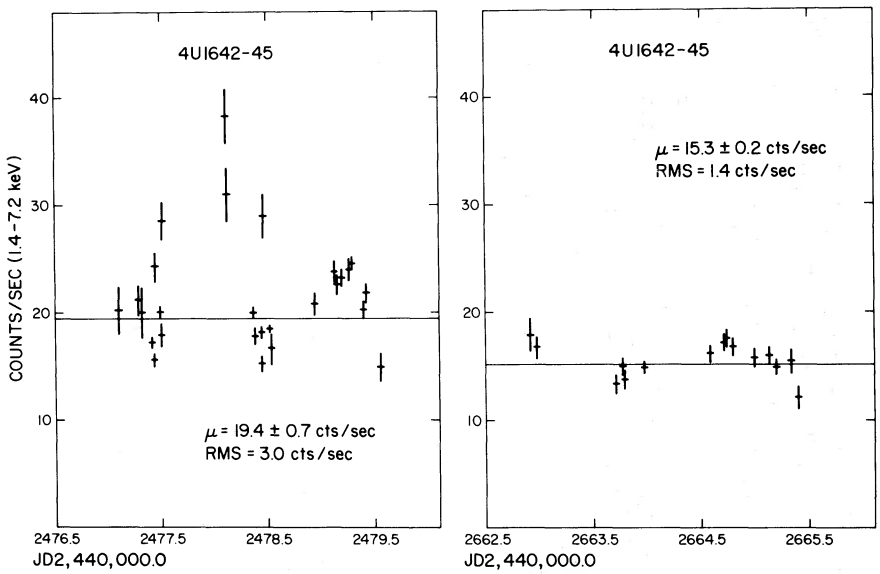

FIG. 1.—X-ray light curves (1.4–7.2 keV) of 4U 1642−45

between 0.93 and 28.1 keV. The PHA has been described elsewhere (Kubierschky *et al.* 1975). The PHA was calibrated on the Crab Nebula, 1975 March 12–15 and September 14–18, and again 1976 March 12–15. The results of the χ^2 fits to a power-type spectrum with a low-energy cutoff are indicated in Table 5E, and show that the LAD was exceptionally stable over the time period of all the *ANS* observations.

We summed all of the available PHA data on a given source in each of the two or three observing periods. Only data taken in relatively low and constant background were used to calculate minimum χ^2 fits of the data to model source spectra. The variable parameters of the fits were (1) a low-energy absorption, (2) a spectral energy index or temperature, and (3) a normalization constant.

The spectral data were fitted to power-law, exponential, and a bremsstrahlung model spectra of the following forms:

Power-law spectrum,

$$dF/dE = A[\exp(-E_a/E)^{8/3}]E^{-\alpha};$$

Exponential spectrum,

$$dF/dE = A[\exp(-E_a/E)^{8/3}]\exp(-E/kT);$$

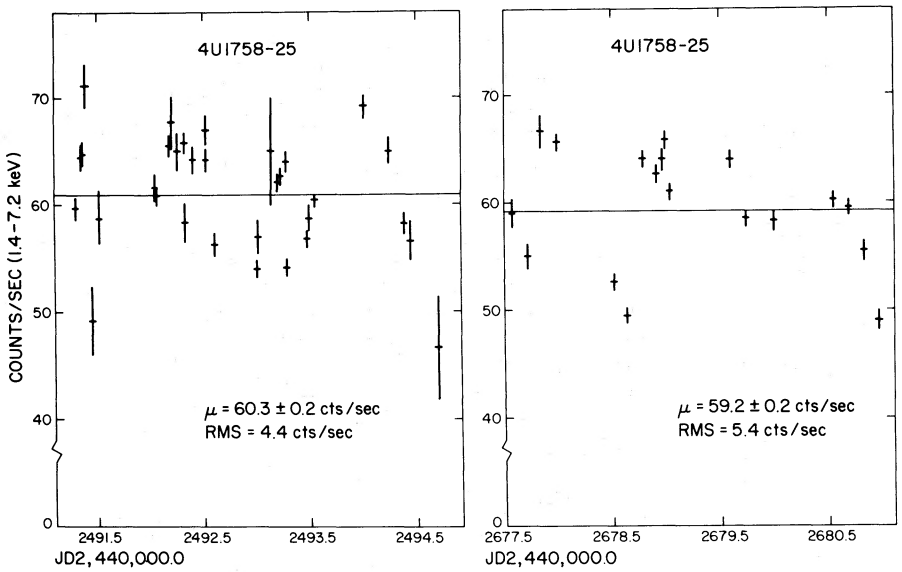

FIG. 2.—X-ray light curves (1.4–7.2 keV) of 4U 1758−25

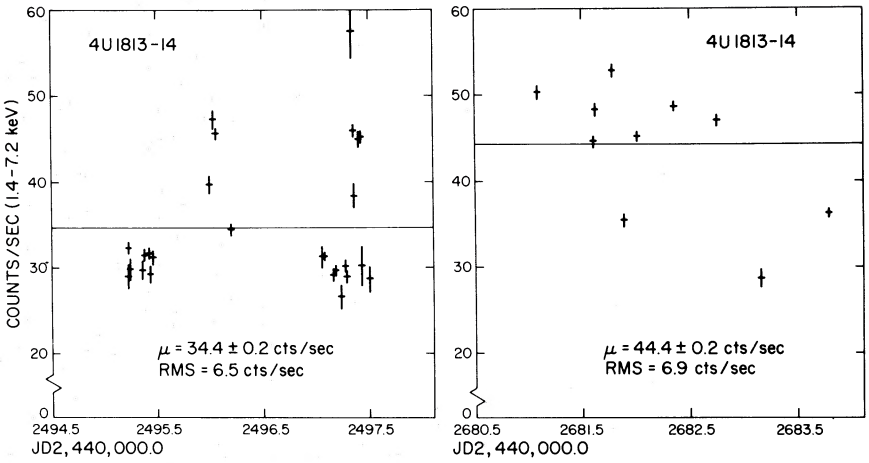

FIG. 3.—X-ray light curves (1.4–7.2 keV) of 4U 1813−14

Bremsstrahlung spectrum,

$$dF/dE = Ag(E, kT)[\exp(-E_a/E)^{8/3}] \exp(-E/kT),$$

where dF/dE is in units of keV cm^{-2} s^{-1} keV^{-1}, and E = energy (keV), E_a = low energy cutoff (keV), α = spectral index, kT = temperature (keV), A = normalization constant (keV cm^{-2} s^{-1} keV^{-1}), and $g(E, kT)$ = Gaunt factor, calculated numerically from the formulation given by Kellogg, Baldwin, and Koch (1975).

From the low-energy cutoffs, we calculated equivalent column densities using the cross sections and abundances given by Brown and Gould (1970).

An analysis of the spectrum of Cygnus X-3 observed by *ANS* had shown a statistically significant excess above the fitted X-ray continuum in two energy channels, between 4.6 and 7.2 keV (Parsignault *et al.*

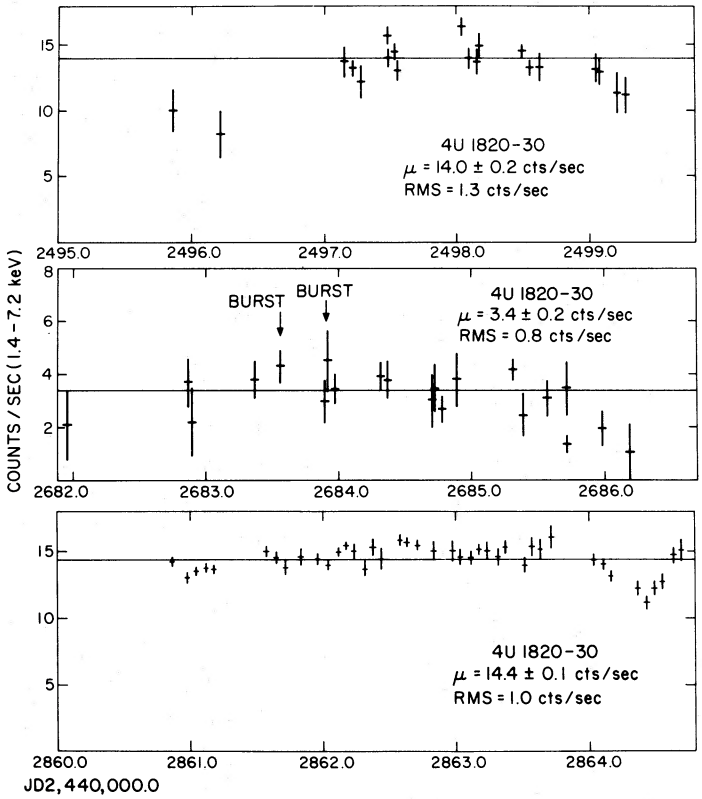

FIG. 4.—X-ray light curves (1.4–7.2 keV) of 4U 1820−30

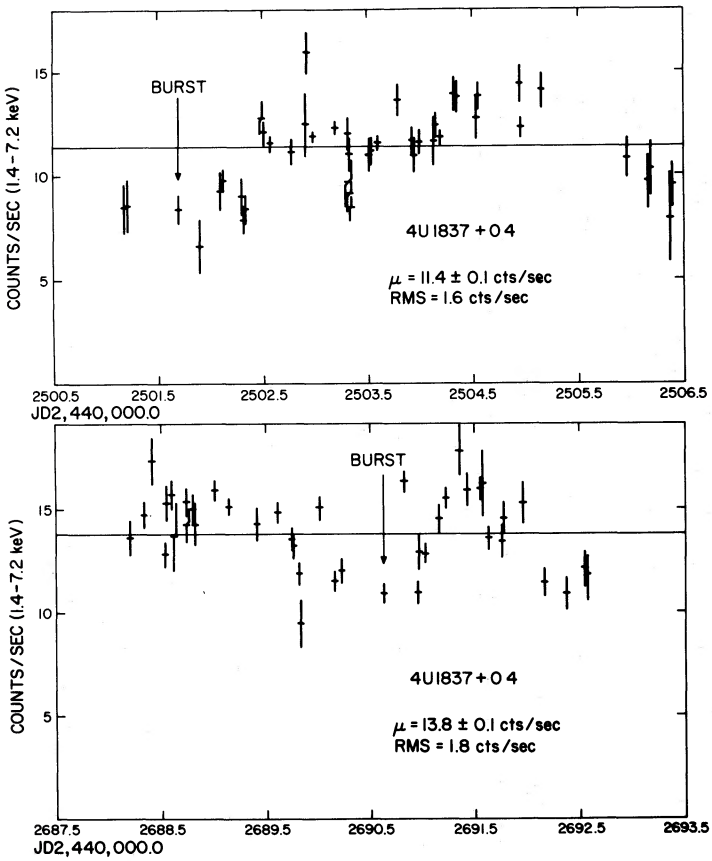

FIG. 5.—X-ray light curves (1.4–7.2 keV) of 4U 1837+04

1977). These results confirmed the findings by two other groups which had identified this same feature as line emission of highly ionized iron (Serlemitsos *et al.* 1975; Sanford, Mason, and Ives 1975). Since most of the 20 sources studied here have intensities comparable to Cyg X-3, we performed a similar search for iron line emission in their spectra. A best-fit continuum spectrum was thus determined with the two PHA channels between 4.6 and 7.2 keV omitted. From the differences between the observed number of counts and the fitted number of counts in these two channels, we calculated the equivalent line widths for Fe line emission. The justification for using this simple method of spectrum analysis is that, in cases where statistically significant ($\gtrsim 3\,\sigma$) flux excesses above the best-fitted continua [$P(>\chi^2) > 10\%$] were observed, leaving out these two channels remarkably improved the χ^2 of the fits over those obtained using all of the 15 PHA channels, while not appreciably changing ($< 1\,\sigma$) the spectrum parameters of the same fits. In the cases where we report a 3 σ upper limit for the iron line, the omission of these two energy channels did not significantly change the fits. The instrumental resolution (~ 1 keV) at the iron line energy does not allow a precise determination of the energy of the observed feature. The line emission could be that of Fe XXVI at 6.93 keV, from recombination of fully ionized iron, or the resonance lines of He-like iron, Fe XXV, from recombination, or the K fluorescence lines from Fe XXIV or lower states. A typical energy spectrum (that of 4U 1744−26) for which iron line analysis was conducted is shown in Figure 7. As discussed below, a statistically significant excess between 4.6 and 7.2 keV is evident above the fitted exponential-type continuum.

In Table 5 we give results of the spectral fits. Table 5A lists the five sources for which significant evidence for Fe line emission was found; Table 5B gives the results for three sources for which Fe line emission may have been detected, although with some degree of uncertainty due to either the poor fit of the continuum or to apparent Fe line variability (e.g., 4U 1820−30); Table 5C includes four sources whose continua are best fitted by an exponential-type spectrum, but for which only upper limits (3 σ) for iron line emission can be inferred; Table 5D lists the remaining sources for which no spectrum preference and no iron line feature could be established. Our calibration spectra on the Crab Nebula are shown in the last section, Table 5E. In this table, column (2) lists the observation periods, for a given observing period, columns (3) through (7) list on the first line

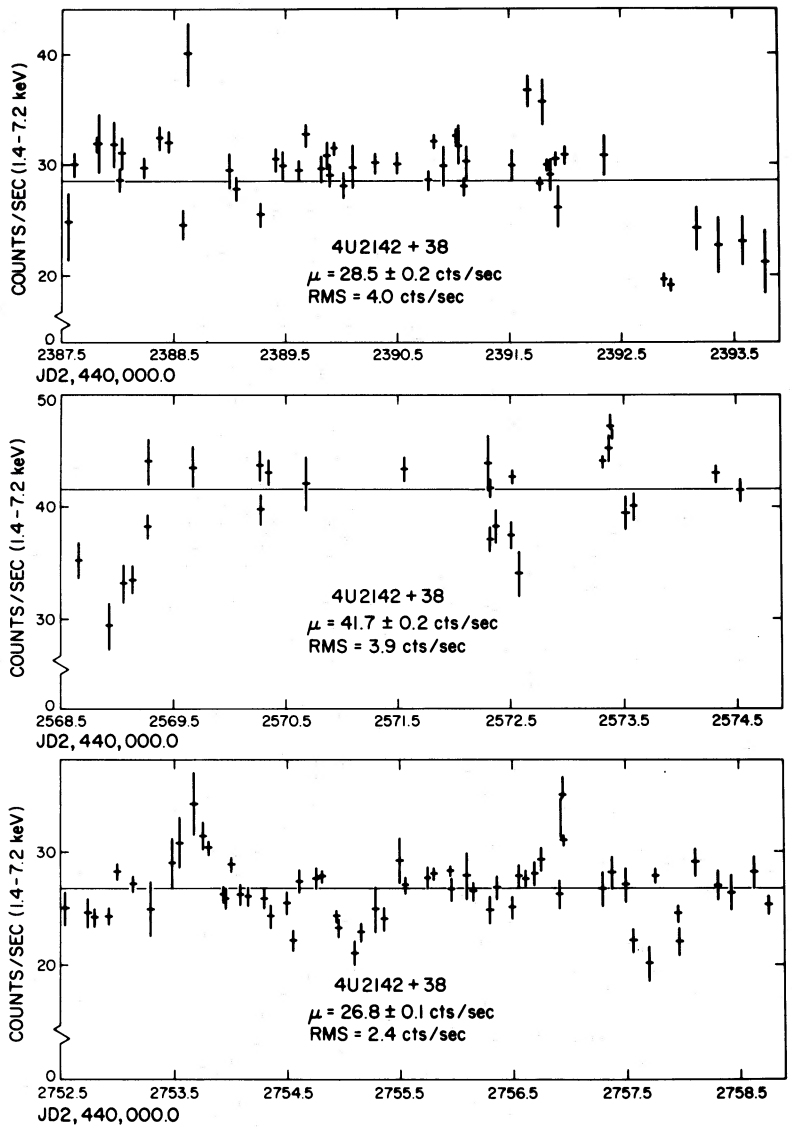

FIG. 6.—X-ray light curves (1.4–7.2 keV) of 4U 2142+38

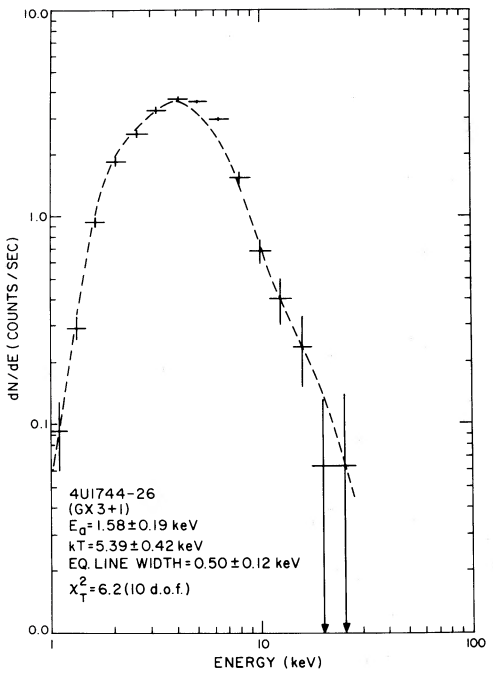

FIG. 7.—Energy spectrum of 4U 1744−26, observed in 1975 September. The horizontal bars represent the observed count rates over the energy intervals. The vertical bars represent $\pm 1\ \sigma$ uncertainties. The dashed line represents the best exponential fit of the observed continuum. A $4\ \sigma$ statistically significant excess above the fitted continuum is apparent in the energy range 4.6–7.2 keV, and is probably due to Fe line emission at ~6.7 keV with an equivalent line width of 0.50 ± 0.12 keV.

the resulting parameters of a spectrum fitted to a power-law–type spectrum: low-energy cutoff, E_a (keV), equivalent column density (atoms cm^{-2}), spectral index α, and equivalent line width (keV), together with the total χ^2 of the fit. The second line of the same observing period lists the same parameters, with α replaced by kT, for an exponential-type spectrum. In the cases where an equivalent line width or upper limit is given, the total χ^2 is for 10 degrees of freedom. If no equivalent width is given, the total χ^2 is for a spectrum fitted with 12 degrees of freedom. The last column gives the average intensities of the observations used in the spectrum data. It should be noted that these intensities are not necessarily equal to the average intensities of the sources over the same observing periods shown in column (3) of Table 1.

Although the total number of parameters in the fitting functions is three (A, E_a, and α or kT), only two parameters (E_a and α or kT) are fitted simultaneously. Thus the errors quoted for these parameters correspond to $\chi^2_{\min} + 2.3$, which corresponds to $\pm 1\ \sigma$ (Avni 1976). In general, the $\chi^2_{\min} + 2.3$ contours were small circles on the χ^2 square grids, centered on the $\chi^2_{\min}$ points. In a few cases, corresponding to low-intensity sources, the contours were ellipsoids, and in such cases we give the values of these ellipsoids projected on the cutoff and spectral-index axes.

We also fitted the observed spectra to a thermal bremsstrahlung-type spectrum, i.e., an exponential-type spectrum plus a Gaunt factor, but we do not list the results in Table 5, since this type of spectrum never significantly improved the fits compared to an exponential-type spectrum: the low-energy cutoffs remained essentially unaffected, while the temperatures increased by about 30 to 70%.

III. DISCUSSION

Interpretation of our study of the time variability and spectra of strong galactic X-ray sources requires a comparison of the results on the different sources as a first step toward their classification. The most obvious comparison of the sources can be made starting with their X-ray spectra. Jones (1977), Ostriker (1977), and Markert *et al.* (1977) have pointed out that the galactic-bulge GX sources considered have characteristic spectra softer than those observed in known X-ray binary systems with supergiant primary components. The differences in the X-ray spectra may be caused by the different accretion mechanisms responsible for the X-ray emission, and by variations in the physical variables of the emitting systems (e.g., accretion rates and flow geometry, electron-scattering optical depths, masses of the collapsed object, or angles of inclination).

We note that while our spectral fits to power-law–type or exponential-type distributions allow some basis of source comparison, the underlying emission process can still be ambiguous. Comptonization of a thermal spectrum can lead to a power-law spectral shape (Shapiro, Lightman, and Eardley 1976). Alternatively, a power-law distribution is often the signature of nonthermal, high-energy electrons revolving in a magnetic field and emitting synchrotron radiation. These electrons can be accelerated by a pulsar (e.g., as in the Crab Nebula), or by magnetohydrodynamical processes in an accretion disk. The interpretation of an exponential-type spectrum, or a thermal bremsstrahlung spectrum which includes the Gaunt factor, can also be ambiguous for determining the X-ray emission mechanism. The emission from a hot thin plasma can result in an exponential distribution of the X-ray continuum if indeed optical depth effects and temperature gradients are not significant in the emission region. However, Hirshfield, Baldwin, and Brown (1961), and Gnedin and Sunyaev (1973) have shown that the spectrum of cyclotron radiation from a thermal plasma can also give an exponential distribution. Finally, there is no reason to expect that only one spectral distribution is produced in a given object; we should rather expect that the observed spectrum is the result of the superposition of several different distributions produced in various regions of the emitting system.

In our present study, eight objects were shown to definitely favor an exponential (or bremsstrahlung) distribution over the range 1–20 keV. A preference for a given distribution was based on the criterion that the χ^2 value of a particular fit was within 90% confidence level for one spectral type while the probability

TABLE 5A

SPECTRAL PARAMETERS FOR SOURCES BEST FITTED BY EXPONENTIAL SPECTRA AND IRON LINE EMISSION

Sources	Obs. Periods JD 2,440,000.0+	E_a (keV)	Column Density (atoms cm^{-2})	α, kT† (keV)	Eq. Width (keV)	χ_T^2	I (counts s^{-1})
4U 1617−15*							
(Sco X-1).....	2466.0–	1.26 ± 0.07	(9.5 ± 0.5) 10^{21}	0.91 ± 0.04	0.64 ± 0.08	80	859
	2470.1	< 0.50	< 1.5 × 10^{21}	7.0 ± 0.4	0.41 ± 0.08	50	
	2652.6–	1.49 ± 0.08	(1.4 ± 0.2) 10^{22}	1.43 ± 0.06	0.59 ± 0.13	50	762
	2654.6	0.69 ± 0.21	(1.9 + 1.6, −0.4) 10^{21}	4.13 ± 0.24	0.34 ± 0.11	24	
4U 1744−26							
(GX 3+1).....	2689.3–	2.75 ± 0.17	(5.3 ± 1.1) 10^{22}	2.21 ± 0.15	< 1.14	20.0	20.0
	2491.7	2.14 ± 0.25	(3.5 ± 1.3) 10^{22}	2.94 ± 0.60	< 0.96	15.3	
	2675.7–	1.98 ± 0.08	(2.7 ± 0.3) 10^{22}	1.20 ± 0.08	0.57 ± 0.13	18.6	22.7
	2678.3	1.58 ± 0.19	(1.7 ± 0.3) 10^{22}	5.39 ± 0.42	0.50 ± 0.12	6.2	
4U 1813−14							
(GX 17+2).....	2495.1–	2.50 ± 0.05	(4.0 ± 0.2) 10^{22}	1.51 ± 0.07	0.62 ± 0.09	35.2	31.2
	2497.7	2.14 ± 0.07	(3.5 ± 0.3) 10^{22}	4.02 ± 0.24	0.32 ± 0.08	30.6	
	2680.9–	2.46 ± 0.07	(5.2 ± 0.4) 10^{22}	1.23 ± 0.07	0.55 ± 0.07	39.4	47.7
	2683.8	2.20 ± 0.09	(3.7 ± 0.5) 10^{22}	5.19 ± 0.38	0.37 ± 0.10	24.6	
4U 2142+38							
(Cyg X-2).....	2387.5–	1.98 ± 0.08	(2.7 ± 0.3) 10^{22}	1.90 ± 0.13	0.71 ± 0.20	16.3	29.3
	2394.7	1.32 ± 0.14	(1.0 ± 0.4) 10^{22}	3.30 ± 0.26	0.55 ± 0.18	13.0	
	2568.6–	2.00 ± 0.05	(2.8 ± 0.2) 10^{22}	1.98 ± 0.07	0.76 ± 0.15	33.7	43.9
	2574.5	1.22 ± 0.10	(8.6 + 1.2, −2.0) 10^{21}	3.19 ± 0.18	0.40 ± 0.12	7.0	
	2752.5–	1.74 ± 0.04	(2.2 ± 0.2) 10^{22}	1.49 ± 0.05	0.38 ± 0.09	59.3	27.4
	2758.8	1.02 ± 0.10	(5.1 + 1.8, −1.5) 10^{21}	4.21 ± 0.19	0.17 ± 0.08	29.4	
4U 1811−17‡							
(GX 13+1).....	2495.2–	3.00 ± 0.14	(6.9 ± 1.0) 10^{22}	2.16 ± 0.17	0.86 ± 0.28	17.3	14.9
	2495.4	2.49 ± 0.17	(4.0 ± 0.8) 10^{22}	3.16 ± 0.47	0.54 ± 0.24	17.1	
	2679.9–	3.05 ± 0.15	(7.3 ± 1.1) 10^{22}	2.48 ± 0.12	0.81 ± 0.36	16.9	13.7
	2683.1	2.70 ± 0.20	(5.0 ± 1.2) 10^{22}	2.36 ± 0.30	0.72 ± 0.34	17.6	

* First set of observations made near satellite apogee (~1100 km), i.e., high radiation environment.

† In each observation throughout Tables 5A–D, the first line refers to a power-law fit and the second line to an exponential fit.

‡ Both exponential and power-law fits acceptable but included in this table since iron line emission is probably always detected.

of occurrence of the value of χ^2 determined for the other spectral fit was < 5%.

Based on that criterion, the X-ray continua of Sco X-1, 4U 1636−53, and 4U 1758−20 were best fitted by an exponential-type spectrum in one set of observations, while 4U 1702−36, 4U 1744−26, 4U 1813−14, 4U 1837+04, and 4U 2142+38 were best fitted by an exponential-type spectrum in two sets of observations made 6 months apart. One should remark in Table 5 that the averaged spectra of 4U 1702−36 (second observing period) and of 4U 1813−14 have unacceptably large χ^2. These sources exhibit a strong temperature-intensity relation in the 1.4–7.2 keV range (see discussion below). Since the averaged spectra for

TABLE 5B

SPECTRAL PARAMETERS FOR SOURCES FITTED BY EITHER EXPONENTIAL OF POWER-LAW SPECTRA AND POSSIBLE IRON LINE EMISSION

Sources	Obs. Periods JD 2,440,000.0+	E_a (keV)	Column Density (atoms cm^{-2})	α, kT† (keV)	Eq. Width (keV)	χ_T^2	I (counts s^{-1})
4U 1642−45							
(GX 340+0).....	2477.1–	3.52 ± 0.08	(1.12 ± 0.08) 10^{23}	2.59 ± 0.05	0.62 ± 0.19	24	18.9
	2479.6	2.92 ± 0.14	(6.4 ± 0.9) 10^{22}	2.84 ± 0.33	< 0.45	30.7	
	2662.9–	3.28 ± 0.16	(9.1 ± 1.3) 10^{22}	1.59 ± 0.09	< 0.60	40	14.9
	2665.5	2.77 ± 0.19	(5.4 ± 1.2) 10^{22}	4.96 ± 0.70	< 0.45	34	
4U 1758−25							
(GX 5−1).....	2491.1–	2.79 ± 0.04	(5.5 ± 0.3) 10^{22}	1.81 ± 0.06	0.47 ± 0.08	52	62.8
	2495.0	2.51 ± 0.05	(4.1 + 1.1, −0.2) 10^{22}	3.34 ± 0.07	0.29 ± 0.07	46	
	2677.5–	2.78 ± 0.03	(5.5 ± 0.2) 10^{22}	1.91 ± 0.04	0.54 ± 0.08	86	59.6
	2681.1	2.44 ± 0.05	(5.1 + 1.1, −0.3) 10^{22}	3.02 ± 0.12	0.23 ± 0.07	66	
4U 1820−30							
(NGC 6624).....	2495.9–	1.40 ± 0.11	(1.3 ± 0.3) 10^{22}	1.12 ± 0.08	0.67 ± 0.17	16.4	14.1
	2499.5	0.67 ± 0.25	(1.8 + 1.9, −0.8) 10^{21}	4.27 ± 0.36	0.62 ± 0.17	9.7	
	2681.9–	< 1.25	< 10^{22}	0.41 ± 0.30	< 1.8	10.3	3.2
	2686.2	< 1.50	< 1.3 × 10^{22}	15.0 ± 7.0	< 1.2	11.3	
	2860.8–	1.25 ± 0.12	(9.3 + 1.6, −3.0) 10^{21}	0.89 ± 0.08	< 0.48	36	14.9
	2864.9	< 0.75	< 3 × 10^{21}	6.91 ± 0.89	< 0.36	31	

TABLE 5C

SPECTRAL PARAMETERS FOR SOURCES BEST FITTED WITH EXPONENTIAL SPECTRA AND NO (3 σ limits) IRON LINE EMISSION

Sources	Obs. Periods JD 2,440,000.0+	E_a (keV)	Column Density (atoms cm^{-2})	α, kT† (keV)	Eq. Width (keV)	χ_r^2	I (counts s^{-1})
4U 1636−53.....	2663.0–	2.03 ± 0.14	(2.9 + 0.7, −0.5) 10^{22}	2.06 ± 0.14	< 1.20	26.0	16.5
	2667.0	1.15 ± 0.27	(7.3 ± 4.4) 10^{22}	2.94 ± 0.48	< 0.90	16.0	
4U 1702−36							
(GX 349+2).....	2479.5–	2.04 ± 0.11	(3.0 ± 0.5) 10^{22}	1.16 ± 0.12	< 0.60	21.9	49.0
	2481.0	1.69 ± 0.15	(2.0 ± 0.6) 10^{22}	5.16 ± 0.68	< 0.52	15.2	
	2667.5–	1.93 ± 0.07	(2.5 ± 0.3) 10^{22}	1.25 ± 0.07	0.39 ± 0.11	51.0	42.3
	2669.0	1.43 ± 0.11	(1.4 ± 0.3) 10^{22}	5.34 ± 0.38	< 0.32	31.5	
4U 1758−20							
(GX 9+1).....	2492.1–	2.51 ± 0.15	(4.1 ± 0.7) 10^{22}	1.70 ± 0.18	< 0.75	24	28
	2495.3	1.97 ± 0.19	(2.7 + 0.8, −0.3) 10^{22}	3.83 ± 0.60	< 0.60	16	
4U 1837+04							
(GX +36.3).....	2500.9–	1.69 ± 0.08	(2.1 ± 0.3) 10^{22}	1.64 ± 0.10	< 0.57	25	10.0
	2506.5	0.66 ± 0.27	(1.7 + 2.1, −0.8) 10^{21}	3.88 ± 0.41	< 0.47	15.6	
	2688.1–	1.74 ± 0.10	(2.3 ± 0.3) 10^{22}	1.48 ± 0.12	0.63 ± 0.21	25	15.2
	2692.7	1.00 ± 0.21	(4.7 + 3.9, −2.0) 10^{21}	4.15 ± 0.45	< 0.54	13	

TABLE 5D

SPECTRAL PARAMETERS FOR SOURCES FITTED BY EITHER EXPONENTIAL OR POWER-LAW SPECTRA AND NO (3 σ limits) IRON LINE EMISSION

Sources	Obs. Periods JD 2,440,000.0+	E_a (keV)	Column Density (atoms cm^{-2})	α, kT† (keV)	Eq. Width (keV)	χ_r^2	I (counts s^{-1})
4U 0614+09...	2494.6–	1.17 (+0.83, −0.92)	(0.8 + 2.0, −0.7) 10^{22}	1.74 ± 0.46	...	12.0	2.5
	2499.1	0.76 (+0.74, −0.51)	(0.3 + 1.1, −0.3) 10^{22}	2.41 ± 0.60	...	12.4	
	2859.8–	1.47 ± 0.21	(1.4 + 0.7, −0.4) 10^{22}	1.62 ± 0.22	< 1.5	17.1	2.1
	2862.9	0.61 (+0.39, −0.36)	(1.3 + 3.5, −1.0) 10^{21}	3.20 ± 0.48	< 1.5	15.9	
4U 1624−49...	2660.0–	4.71 ± 0.23	(2.7 ± 0.4) 10^{23}	3.38 ± 0.70	...	16.9	3.3
	2663.6	3.94 ± 0.43	(1.6 ± 0.5) 10^{23}	2.27 ± 0.51	...	18.5	
4U 1728−16							
(GX 9+9).....	2484.3–	1.75 ± 0.15	(2.2 + 0.1, −0.5) 10^{22}	1.53 ± 0.17	< 0.86	13.3	14.2
	2486.5	0.97 ± 0.31	(4.3 + 5.8, −2.7) 10^{21}	4.07 ± 0.75	< 0.81	15.5	
	2671.0–	1.73 ± 0.11	(2.2 ± 0.40) 10^{22}	1.38 ± 0.12	< 0.57	5.9	13.4
	2673.7	0.88 ± 0.28	(3.3 + 3.2, −1.6) 10^{21}	4.63 ± 0.75	< 0.52	9.2	
4U 1728−24							
(GX 1+4).....	2485.2–	1.53 ± 1.25	(1.5 + 3.2, −1.2) 10^{22}	0.2 ± 0.7	...	10	5.6
	2487.2	1.44 (+1.10, −1.19)	(1.3 + 3.2, −1.1) 10^{22}	> 30	...	10	
	2671.2–	2.75 (+1.25, −1.75)	(5.4 + 10.0, −4.4) 10^{22}	0.6 ± 0.7	...	15.5	2.0
	2673.6	2.50 ± 0.75	(4.0 + 4.5, −1.5) 10^{22}	12 ± 8	...	14.7	
4U 1728−33							
(GX 354+0)...	2670.9–	2.00 (+0.75, −1.75)	(2.7 + 2.7, −2.4) 10^{22}	1.12 ± 0.48	...	23.7	3.2
	2674.3	1.50 ± 0.75	(1.30 + 2.5, −1.3) 10^{22}	6.3 ± 4.1	...	23.9	
	2850.0–	2.26 ± 0.14	(4.1 ± 0.8) 10^{22}	0.88 ± 0.13	...	10.0	7.0
	2852.7	1.97 ± 0.17	(2.7 + 0.7, −0.2) 10^{22}	7.09 ± 1.30	...	7.7	
4U 1735−44...	2674.4–	1.78 ± 0.17	(2.4 + 0.21, −0.63) 10^{22}	1.26 ± 0.16	< 0.90	16.7	10.0
	2675.9	1.12 ± 0.42	(6.7 + 8.8, −4.6) 10^{21}	5.21 ± 0.85	< 0.78	10.4	
4U 1755−33							
(GX −2.5)....	2491.3–	< 1.75	< 2.2 × 10^{22}	1.6 (+0.7, −0.3)	...	16.1	3.6
	2492.5	< 1.25	< 10^{22}	2.2 ± 0.6	...	15.9	
	2679.5–	2.0 ± 0.5	(2.9 ± 0.9) 10^{22}	2.1 ± 0.8	...	20.8	3.6
	2680.8	1.7 ± 0.5	(2.1 ± 1.5) 10^{22}	2.3 ± 0.5	...	19.6	

TABLE 5E

SPECTRAL PARAMETERS FOR POWER-LAW FITS TO CALIBRATION SOURCE

Sources (1)	Obs. Periods JD 2,440,000.0+ (2)	E_a (keV) (3)	Column Density (atoms cm^{-2}) (4)	α (5)	χ_r^2 (6)	I (counts s^{-1}) (7)
4U 0531+21						
(Crab Nebula)...	2484.4–2488.5	0.42 ± 0.40	(1.06 + 2.13, −1.05) 10^{21}	1.10 ± 0.07	4.9	64.2
	2671.1–2675.3	0.57 ± 0.29	(1.07 + 2.68, −0.78) 10^{21}	1.09 ± 0.04	14.3	64.5
	2851.9–2852.1	0.95 ± 0.07	(4.1 + 1.0, −0.9) 10^{21}	1.19 ± 0.04	15.1	64.8

these sources were obtained from observations made over a wide range of intensities, these large χ^2 values are most probably due to the variations in kT with intensity. The preference for an exponential distribution was established from summed spectral data at given intensities, rather than from the total spectral data shown in Table 5.

The observed range of temperatures was 2.9–7.7 keV. The interpretation of thermal bremsstrahlung emission is further strengthened by the observation of Fe line emission in several of these objects: 4U 1617−15, 4U 1744−26, 4U 1813−14, and 4U 2142+38. One object, 4U 1811−17, for which we could not distinguish between the two spectral types but which also exhibited iron line emission features (at $>2\,\sigma$ level), most probably can be classified with the above eight sources. Since iron line emission was probably detected in the first observing period of 4U 1820−30 (but *not* in the third) during its high (nonbursting) state, it may sometimes also be a thermal source during this phase. The object 4U 1642−45 (power-law–type spectrum only) and 4U 1758−25 (both spectrum types) also showed significant ($>3\,\sigma$) excess emission at ∼6.7 keV above the best-fit continuum spectra. However, since the χ^2 values of these fits were very large [$P(>\chi^2) \ll 5\%$] and no satisfactory continuum fits could be obtained (either with or without the two PHA channels between 4.6 and 7.2 keV), we must regard the origin of the apparent excess flux in these channels as uncertain. No sources were found for which a power-law–type spectrum alone fitted the data, although for many sources this type of spectrum could not be excluded: 4U 0614+09, 4U 1728−33, 4U 1728−16, 4U 1728−24, 4U 1735−44, 4U 1755−33, 4U 1811−17, and 4U 1820−30.

Contrary to the results of similar analysis performed on the spectra of all other objects, we found in the case of Sco X-1 a significant deviation ($3.2\,\sigma$) in the PHA channel (energy range 7.2–9.0 keV) adjacent to those normally containing the iron line feature. We also found a significant excess ($\gtrsim 3\,\sigma$) in the two channels straddling the iron line (4.6–7.2 keV). The *OSO 8* observers (Serlemitsos 1977) have also reported for Sco X-1, over about the same energy range of 4.6–9.0 keV, a similar large excess flux above the fitted X-ray continuum, with a resulting equivalent line width of ∼1.0 keV. We derive an equivalent line width of ∼0.7 keV for this broadened iron line feature, with an estimated width (FWHM) of ∼2 keV.

We have calculated the line-to-continuum power ratios for the different sources for which we observed a statistically significant excess above the fitted continuum, at ∼6.7 keV, and compared them to the calculations of Mewe (1972). This author calculated line-to-continuum ratios as a function of temperature making certain assumptions which should be acceptable for a quiet or moderately active solar corona. While we realize that these conditions are probably not satisfied for the objects considered here, Mewe's calculations and our observed line-to-continuum ratios may nevertheless give an indication of the Fe abundance in the X-ray sources. The ratios found for Sco X-1, 4U 1744−26, 4U 1811−17, and 4U 1820−30 indicated that the Fe abundances in these objects are marginally below the cosmic value, $N(\mathrm{Fe})/N(\mathrm{H}) = 5 \times 10^{-5}$. In the case of 4U 1813−14 (GX 17+2), both sets of measurements indicated an Fe abundance about one-third the cosmic value. As for 4U 2142+38, we found a variable Fe line emission feature which yielded abundance ratios $N(\mathrm{Fe})/N(\mathrm{H})$ which varied from ∼6% to 100% of the cosmic value.

A further classification can be made using the intensity-temperature correlation (or lack thereof). Figure 8 shows these relationships in sources for which data were available for such analysis. The bars on each point represent $\pm 2\,\sigma$ uncertainties. Sources with a direct correlation between kT and I may be similar to Sco X-1, which also shows this relation (White *et al.* 1976). We observed the temperature to increase with intensity on a short time scale (∼hours) for 4U 1702−36, 4U 1744−26, and 4U 1813−14, and on a long time scale (∼6 months) for Sco X-1 and 4U 1728−24. Mason *et al.* (1976) reported such behavior on a time scale of ∼hours for 4U 1702−36, 4U 0614+09, Sco X-1, 4U 1728−16, and 4U 1758−25. The conditions of our observations of 4U 0614+09 and Sco X-1 (i.e., approximately constant intensity) did not allow us to verify this relation on short time scales. In the case of 4U 1728−16, the intensity range of our observations corresponds to the ∼72–85 counts per 62.5 s intensity range of *Copernicus*. Over this range we do not see the intensity-temperature correlation reported by Mason *et al.* (compare our Fig. 8*c* with Fig. 2 in Mason *et al.* 1976). The intensity range over which our observations of 4U 1758−25 were made corresponds to ∼268–356 counts per 62.5 s of *Copernicus*. Over this range, the temperature is constant, in agreement with the observations of Mason *et al.* The three sources for which we find a direct intensity-temperature relation show large changes in intensity over a period of one to several hours, as well as days. The source 4U 1758−20, for which no such correlation was found over the observed intensity range, may be of the same type since it showed large intensity variations over the same time scales.

In addition to being the highest temperature source detected, 4U 1728−24 stands out in this survey as almost certainly (given its 122 s pulsations) a close binary system. The long-term positive correlation between source temperature and intensity, the large low-energy cutoff, and the high temperature of the spectrum closely resemble the properties of the known close binary systems (e.g., Cen X-3, Her X-1, SMC X-1, and 4U 0900−40).

Over the intensity ranges shown in Figure 8, no intensity-temperature relations were found for 4U 1728−33 and 4U 1837+04. In the case of 4U 1642−45, spectral data were not available at the intensity extremes, but only at $I \approx 19$ counts s^{-1} (first period) and $I \approx 15$ counts s^{-1}, 6 months later. Thus, on a time scale of ∼hours, the temperature-intensity relation could not be established from our data. A similar remark applies to Cyg X-2.

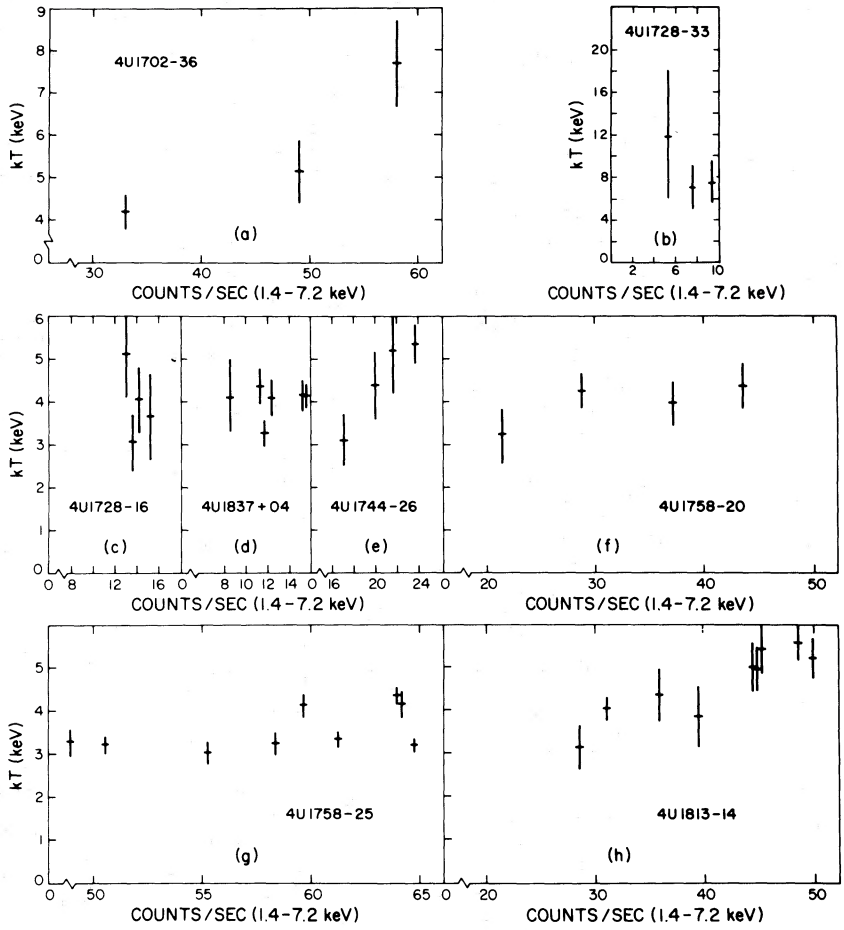

FIG. 8.—Temperature (kT) of the best-fit exponential spectrum vs. source intensity (1.4–7.2 keV) observed for 4U 1702−36, 4U 1728−16, 4U 1728−33, 4U 1744−26, 4U 1758−20, 4U 1758−25, 4U 1813−14, and 4U 1837+04. The error bars represent $\pm 2\,\sigma$ uncertainties.

A long-term intensity-temperature relation was found for 4U 1642−45, 4U 1820−30, and 4U 2142−38 (Cyg X-2), and a short-term one (during intensity dips) for 4U 1837+04 whereby the temperature increased with decreases in the average intensity while the low-energy cutoff remained essentially unchanged. This intensity-temperature relation is characteristic of sources such as Cyg X-3 (Parsignault *et al.* 1977) or Cyg X-1 during its transition phases (Heise *et al.* 1975; Parsignault *et al.* 1975). However, the four sources noted here are differentiated from one another by their time variability (cf. Tables 2–4 and discussion below). Note that in the case of 4U 1642−45 this correlation is not affected by the poor χ^2 value of the spectral fits since this result could equally well be expressed as a change in the sources' "hardness ratio" (i.e., ratio of high- to low-energy flux of the sources).

The source 4U 1642−45 was the most active source in our survey on all time scales considered. Forman, Jones, and Tananbaum (1976) have also observed activity for this object which was not unlike that of Cyg X-3. These authors observed that the intensity of 4U 1642−45 appeared to be modulated with a period of ~ 1.5 days, but such modulation was not always present in the *Uhuru* data and is not present in the *ANS* data.

The behavior of 4U 1642−45 can be contrasted to that of 4U 1820−30, 4U 1837+04, and 4U 2142+38, which, although showing occasional large isolated transitions on the same time scales, tend to be more constant on the average. Except for large changes in intensity on a 6 month time scale, Cyg X-2 was, together with 4U 1758−25, the most constant source observed in our survey of 20 sources (cf. Table 4). The mean intensity fluctuations of 4U 1820−30 were average on time scales between 1 s and 20 min, below average on longer time scales ($\lesssim 1$ day), and significantly above average on a 6 months' time scale. On the other hand, 4U 1837+04 had mean fluctuations slightly above the average for all time scales $\lesssim 1$ day and also showed above average transitions on a 6 month time scale.

The source 4U 1837+04 can be singled out by the observation of fast decreases in its intensity which are

accompanied by hardening of the X-ray spectrum. These dips in intensity occurred on JD 2,442,503.2 and 689.7. No spectral data were available during the first event, during which the intensity changed from 12 to 8.4 counts s^{-1} in ~ 15 min. However, the second dip showed a spectral hardening as the intensity decreased, with E_a remaining constant. As the intensity decreased from 14.8 to 10 counts s^{-1}, over a period of ~ 110 min, the kT increased from 3.70 ± 0.44 keV to 6.9 ± 2.0 keV. Such a behavior had previously been observed in Cyg X-1 (Li and Clark 1974; Mason *et al.* 1974; Parsignault *et al.* 1975; Parsignault *et al.* 1976). In Cyg X-1, the sharp intensity dips are correlated with the binary phase. Therefore 4U 1837+04 could be a member of a close binary system although no periodicities $\lesssim 2$ days were observed. The dips found in the spectrum of 4U 1837+04 could as well be due to sudden increases in the Comptonization (by unsteady accretion yielding sudden changes in optical depth) of a soft spectrum.

Finally, these four sources for which an inverse correlation between intensity and temperature was found have one other point in common insofar as they exhibit large changes in their average intensities on a 6 month time scale.

We have examined the data for *all* sources observed for possible correlations between both apparent source flux and/or approximate X-ray "luminosity" (i.e., the quantity $n_H{}^2 I$, since this would be proportional to luminosity if the column density were a measure of distance only) and the rms percentage fluctuation intensity. No obvious correlations were found. Correlation is also not evident between source spectral temperature and rms fluctuation intensity.

We may also compare all of our results for the five candidate steady-source counterparts of X-ray bursters observed in this study: 4U 1636−53, 4U 1728−33, 4U 1735−44, 4U 1820−30, and 4U 1837+04. With the exception of 4U 1820−30, for which the identification of the burster with the steady source is certain (Grindlay *et al.* 1976; Clark *et al.* 1977), the other burster identifications are based solely on a coincidence of $\sim 5'$–$10'$ burster positions with the steady source positions (cf. Lewin 1977). We assume that these identifications are probably correct, and that X-ray bursts are unique to a class of X-ray sources and are not an incidental or occasional characteristic shown by all of the galactic-bulge X-ray sources. Comparison of our spectral and variability (of the associated persistent sources) results for bursters leads to this assumed distinction:

The results summarized in Tables 1–5 and the discussion above show first that none of the bursters (at least) during burst-active periods (e.g., 4U 1820−30 in low state) seem to have iron line emission in their spectra, although the spectra of 4U 1636−53 and 4U 1837+04 appear to be thermal. As noted above, however, several of the equivalent line width upper limits are above most of our other measured values and so may be of limited significance. Second, we note that at least two of these sources (4U 1820−30 and 4U 1837+04) show an inverse correlation between intensity and spectral hardness. A direct correlation of kT versus I as for Sco X-1–type sources was *not* observed for the possible burster counterparts. Finally, the two largest transitions in average flux intensity (averaged over several days) between the observing periods with 6 month separation were found for 4U 1636−53 and 4U 1820−30. In general, comparison of the source variability results of Tables 2–4 suggests that the bursters showed larger maximum flux transition on time scales ≥ 3 hours–6 months than the remaining sources. However, we do not find any significant differences in the fractional power contained in 0.1 s–16 s fluctuations of the continuous emission from these sources as compared to the other sources in our study.

IV. CONCLUSIONS

We summarize our major conclusions as follows:

1. Most GX sources are best fitted in the ~ 1–20 keV range by exponential spectra with $kT \approx 5$ keV. However, for some sources (e.g., 4U 1642−45 and 4U 1758−25) the poor fits to simple exponential or power-law–type distributions indicate a more complex spectrum. Poor fits (i.e., complex spectra) are also sometimes obtained for some sources (4U 1820−30) which at other times are well described by exponential or power-law forms. In other cases (e.g., 4U 1702−36 or 4U 1813−14) poor average spectral fits are due to spectral variability correlated with intensity changes.

2. Iron line emission at ~ 6.7 keV is always detected as a persistent spectral feature of 4U 1617−15, 4U 1744−26, 4U 1813−14, 4U 2142+38, 4U 1642−45, 4U 1811−17, and possibly 4U 1758−25. All of these except Cyg X-2, 4U 1642−45, and 4U 1811−17 are observed either in our study or in that of Mason *et al.* (1976) to show a direct correlation between the source temperature, kT, and the intensity, I, in the 1.4–7.2 keV band.

3. No burst source counterparts (or candidates) showed a direct correlation between kT and I; at least two showed an inverse correlation. No iron line emission was detected at a 3σ level from burster counterparts during burst-active states.

4. Sources showing either direct kT versus I correlation or iron line emission are generally less variable on a time scale of $\gtrsim 3$ hours–6 months than either the burster counterparts or sources with an inverse kT versus I correlation.

5. None of the sources in this study (excluding the known slow pulsar 4U 1728−24) showed any evidence for periodicities with modulation $\gtrsim 10\%$–30% from ~ 2 s to 2 days, respectively.

The above conclusions suggest that the strong X-ray sources in the galactic bulge (GX sources), which have previously been grouped together as having similar luminosities ($\geq 10^{37}$ ergs s^{-1}), similar soft spectra ($kT \approx 5$ keV), and a lack of periodicities (i.e., we exclude pulsars like 4U 1728−24 with a hard spectrum characteristic of known high-mass binaries;

Jones 1977), may be further divided into at least two classes: *class 1 GX sources*, with direct kT versus I correlation, usually fitted with an exponential spectrum plus an iron line emission feature, fluctuating primarily on time scales of minutes to hours; *class 2 GX sources*, with inverse (or no) kT versus I correlation; some (sometimes) are fitted by a power-law spectrum, usually have no iron line emission, and are generally active on all time scales, especially on $\gtrsim 3$ hour, ~ 1 day, and 6 month time scales.

We may thus identify the sources in our survey with these classes: 4U 0614+09, Sco X-1, and Cyg X-2, all of which also have somewhat similar optical counterparts, are then class 1 GX sources. Cyg X-2 is somewhat debatable as a class 1 source on the basis of our data in that it showed an inverse kT versus I correlation over a 6 month period; on short ($\sim$hours) time scales the kT versus I correlation is not yet determined. Additional class 1 GX sources identified with certainty (i.e., all criteria satisfied) are 4U 1744−26 and 4U 1813−14. The class 2 GX sources in this study are then the bursters or at least their candidate steady-source counterparts. To this we could add 4U 1642−45, which shows all the above defining characteristics for class 2 GX sources although its true spectral shape could not be determined from our data.

The remaining sources in our survey are more difficult to classify on this scheme since all the above criteria may not be satisfied (although "opposite" criteria are not satisfied). Nevertheless, we can probably assign—with decreasing probability—4U 1702−36, 4U 1728−16, 4U 1811−17, 4U 1758−20, and 4U 1758−25 all to class 1 as they show most class 1 (but not class 2) characteristics. Classification of 4U 1758−25 is more uncertain since it is conspicuous for its relative *lack* of variability on any time scale and peculiar spectrum which could not be fitted ($\sim$1–20 keV) by any simple form. We are unable to classify 4U 1624−49, 4U 1658−48, and 4U 1755−33 because of their lower flux and hence poorly determined variability and spectrum parameters.

Finally, we comment briefly on the implications of our proposed classification scheme for source models. Class 1 GX sources, if all similar to the prototype objects here (i.e., 4U 0614+09, Cyg X-2, and Sco X-1), may thus be identified with low-mass binary systems. Both the lack of periodicities and presence of relatively constant variability down to $\sim$second time scales could be due to scattering of the X-rays (from an accretion disk around a neutron-star binary companion) by a hot gas cloud enveloping the entire system. The cloud itself would be a significant source primarily responsible for the iron line emission. The "cocoon" model for Cyg X-3 of Milgrom and Pines (1977) is somewhat relevant, although Cyg X-3 shows an *inverse* kT versus I relation (Parsignault *et al.* 1977). Detailed calculations of such a cocoon model for the class 1 GX sources should include the spectral and temporal results presented here. The direct temperature-intensity correlation for class 1 sources may be the signature of a quasi-blackbody ($T \propto I^{\gamma}$, $\gamma \approx$ 0.25–1) or thermal accretion disk since the iron line emission is thermal and all of the known binary (e.g., Sco X-1) GX sources which are thus most likely to contain accretion disks are class 1.

Class 2 GX sources include the burster counterparts, although we do not claim that all class 2 sources must show burst behavior. Indeed, Cyg X-1 shows several characteristics of a class 2 GX source, but produces flarelike behavior as contrasted with the usual behavior of a burster (Canizares and Oda 1977). It will be interesting, nevertheless, to search for both bursts from suspected class 2 GX sources (e.g., 4U 1642−45) and for class 2 characteristics of other steady-source counterparts of bursters.

A model for bursters and their steady emission sources that is consistent with the class 2 definition proposed here has been developed by Grindlay (1978). In this model the observed flux at ~ 5 keV is due to Comptonization of a central blackbody (approximate) source at $\lesssim 1$ keV by a surrounding ($\sim 10^8$ cm) high-temperature ($\gtrsim 100$ keV) source. The Compton optical depth is typically $\tau \lesssim 1$ so that only a few scatterings are involved and time scales $\lesssim 0.1$ s are preserved. The relatively larger changes in steady emission on long time scales ($\gtrsim 3$ hours–6 months) for the class 2 sources may reflect the relatively large changes in average accretion rate responsible for burst-active periods. Since there is no thermal gas at ~ 6 keV in the source region, iron line emission is not expected. X-ray (and γ-ray or ~ 200 keV) bursts can be produced in such a model by the collapse of a constant-density gas shell at $r \approx 10^{10}$ cm formed (for a critical range of accretion rates or luminosities) by X-ray heating. It is possible that searches for iron line emission in the bursts themselves or their associated steady sources (during burst-active states) could test various models since the neutron-star binary models (e.g., Lamb *et al.* 1977) would usually predict thermal plasmas (and thus iron line emission) in an accretion disk at the ~ 5 keV "temperature" observed for class 2 sources.

Future observations can confirm whether GX sources can indeed be classified by their apparent spectral shapes and characteristic time scales for variability as we have proposed. The *HEAO 1* experiments should be able to extend this analysis greatly when pointed observations are eventually carried out, and actual power spectra (versus our pseudo power spectra of Table 3) can be measured from milliseconds to $\sim$hours, and on much lower intensity sources. Complementary spectra over a broad range ($\sim$1–100 keV) are also needed and may again be available for many sources from the *HEAO 1* experiments.

We thank H. Gursky, A. Epstein, E. Schreier, and H. Schnopper for their role in carrying out the observations reported here, and R. Hauck and D. Erb for programming assistance. This work was partially supported by NASA contract NAS5-23282.

REFERENCES

Avni, Y. 1976, *Ap. J.*, **210**, 642.
Becker, R. H., Boldt, E. A., Holt, S. S., Pravdo, S. H., Rothschild, R. E., Serlemitsos, P. J., and Swank, J. H. 1976, *Ap. J.* (*Letters*), **207**, L167.
Brown, R. M., and Gould, R. J. 1970, *Phys. Rev. D.*, **1**, 2252.
Canizares, C. R. 1975, *Ap. J.*, **201**, 589.
Canizares, C. R., and Oda, M. 1977, *Ap. J.* (*Letters*), **214**, L119.
Clark, G. W., Li, F. K., Canizares, C. R., Hayakawa, S., Jernigan, J. G., and Lewin, W. H. G. 1977, *M.N.R.A.S.*, **179**, 651.
Cruddace, R., Bowyer, S., Lampton, M., Mack, J., and Margon, B. 1972, *Ap. J.*, **174**, 529.
Davidson, A., Malina, R., Smith, H., Spinrad, H., Margon, B., Mason, K., Hawkins, F., and Sanford, P. 1974, *Ap. J.* (*Letters*), **193**, L25.
Forman, W., Jones, C., and Tananbaum, H. 1976, *Ap. J.*, **208**, 849.
Giacconi, R., Murray, S., Gursky, H., Kellogg, E., Schreier, E., Matilsky, T., Koch, D., and Tananbaum, H. 1974, *Ap. J. Suppl.*, **27**, 37.
Gnedin, Y., and Sunyaev, R. 1973, *Astr. Ap.*, **25**, 233.
Grindlay, J. 1978, *Ap. J.*, **221**, 234.
Grindlay, J., Gursky, H., Schnopper, H., Parsignault, D. R., Heise, J., Brinkman, A. C., and Schrijver, J. 1976, *Ap. J.* (*Letters*), **205**, L127.
Gursky, H., Schnopper, H., and Parsignault, D. R. 1975, *Ap. J.* (*Letters*), **201**, L127.
Heise, J., Brinkman, A. C., Schrijver, J., Mewe, R., den Boggende, A., Gronenschild, E., Parsignault, D., Grindlay, J., Schreier, E., Schnopper, H., and Gursky, H. 1975, *Nature*, **256**, 107.
Hirshfield, J., Baldwin, D., and Brown, S. 1961, *Phys. Fluids*, **4**, 198.
Holt, S. S., Boldt, E. A., Serlemitsos, P. J., and Kaluzienski, L. J. 1976, *Ap. J.* (*Letters*), **205**, L143.
Janes, A. F., Pounds, K. A., Ricketts, M. J., Willmore, A. P., and Morrison, L. V. 1972, *Nature*, **235**, 152.
Jones, C. 1977, *Ap. J.*, **214**, 856.
Kellogg, E., Baldwin, J. R., and Koch, D. 1975, *Ap. J.*, **199**, 299.
Kubierschky, K., Jagoda, N., Austin, G. K., Parsignault, D. R., Frank, R., and Ballas, J. S. 1975, *IEEE Trans. Nucl. Sci.*, **NS-22**, 551.
Kunkel, W., Osmer, P., Smith, M., Hoag, H., Schroeder, D., Hiltner, W. A., Bradt, H., Rappaport, S., and Schnopper, W. H. 1970, *Ap. J.* (*Letters*), **161**, L169.
Lamb, F. K., Fabian, A. C., Pringle, J. C., and Lamb, D. Q. 1977, *Ap. J.*, **217**, 197.
Lewin, W. H. G. 1977, *M.N.R.A.S.*, **179**, 43.
Li, F. R., and Clark, W. G. 1974, *Ap. J.* (*Letters*), **191**, L27.
Margon, B., and Ostriker, J. P. 1973, *Ap. J.*, **186**, 91.
Markert, T. H., Canizares, C. R., Clark, G. W., Hearn, D. R., Li, F. K., Sprott, G. F., and Winkler, P. F. 1977, *Ap. J.*, **218**, 801.
Mason, K. O., Charles, P. A., White, N. E., Culhane, J. L., Sanford, P. W., and Strong, K. T. 1976, *M.N.R.A.S.*, **177**, 513.
Mason, K. O., Hawkins, F. J., Sanford, P., Murdin, P., and Savage, A. 1974, *Ap. J.* (*Letters*), **192**, L65.
Mewe, R. 1972, *Solar Phys.*, **22**, 459.
Milgrom, M., and Pines, D. 1977, preprint.
Ostriker, J. P. 1977, *annals. NY Acad. Sci.*, **302**, 229.
Parsignault, D. R., Epstein, A., Grindlay, J., Schreier, E., Schnopper, H., Gursky, H., Tanaka, Y., Brinkman, A. C., Heise, J., Schrijver, J., Mewe, R., Gronenschild, E., and den Boggende, A. 1976, *Ap. Space Sci.*, **42**, 175.
Parsignault, D. R., Grindlay, J., Gursky, H., and Tucker, W. 1977, *Ap. J.*, **218**, 232.
Parsignault, D. R., Grindlay, J. E., Schnopper, H., Schreier, E. J., and Gursky, H. 1975, NASA SP-389, p. 429.
Sanford, P. W., Mason, K. O., and Ives, J. 1975, *M.N.R.A.S.*, **173**, 90.
Serlemitsos, P. J. 1977, private communication.
Serlemitsos, P. J., Boldt, E. A., Holt, S. S., Rothschild, R. E., and Saba, J. L. 1975, *Ap. J.* (*Letters*), **201**, L9.
Shapiro, S. L., Lightman, A. P., and Eardley, D. M. 1976, *Ap. J.*, **204**, 187.
White, N. E., Mason, K. O., Sanford, P. W., Ilovaisky, S. A., and Chevalier, C. 1976, *M.N.R.A.S.*, **176**, 91.
Willmore, A. P., Mason, K. O., Sanford, P. W., Hawkins, F. J., Murdin, P., Penston, M. W., and Penston, M. 1974, *M.N.R.A.S.*, **169**, 7.

J. E. GRINDLAY and D. R. PARSIGNAULT: Center for Astrophysics, Harvard College Observatory and Smithsonian Astrophysical Observatory, 60 Garden Street, Cambridge, MA 02138